Amplitude-modulated indirect pumping of spin orientation in low-density cesium vapor

R. Gartman and W. Chalupczak
National Physical Laboratory, Hampton Road, Teddington TW11 0LW, United Kingdom
(Received 5 March 2015; published 26 May 2015)

A recently demonstrated technique of continuous indirect pumping enables a high level of atomic spin polarization to be generated in thermal alkali-metal vapors, without compromising the coherence lifetime through power broadening from the pump laser. The indirect pumping process combines optical excitation and spin-exchange collisions. Here we describe the pumping process and the role of spin-exchange collisions for the case of amplitude-modulated optical excitation. We demonstrate that effective spin-exchange decoherence is modified by the measurement geometry and dynamics. Decoherence changes are studied through magneto-optical-rotation signals. The studies presented here are particularly important for optimizing the performance of an atomic magnetometer operating in the quantum nondemolition configuration in a nonzero-magnetic-field environment.

DOI: 10.1103/PhysRevA.91.053419 PACS number(s): 32.80.Xx, 07.55.Ge, 32.70.Jz

I. INTRODUCTION

Coherence lifetime is one of the parameters that limits the fundamental sensitivity of atomic sensors [1]. In the field of thermal alkali-metal atomic vapors the actual value of the coherence lifetime is set by the spin-exchange collisions (SECs). Standard strategies to eliminate or reduce SEC decoherence rely on coherence transfer [2–4] and optical pumping into a stretched state [5–9], i.e., the state with maximum or minimum quantum number m. The former strategy benefits from prolonged coherent oscillations at a given frequency for the case when the difference between coherence oscillation frequencies before and after SEC is smaller than the relaxation rate [3]. The latter strategy (sometimes referred to as light narrowing [5]) is a consequence of the total angular momentum conservation in SEC processes, which forbids two atoms, both in stretched states, from collisionally changing their internal states.

The usual method for pumping alkali-metal atoms into the stretched state employs a circularly polarized laser beam operating on the $D1$ line [10]. One serious consequence of this approach is the power broadening that affects the coherence lifetime arising from the resonant optical interaction with relevant states [11,12]. Recently, a novel indirect way of pumping into the stretched state without additional power broadening has been demonstrated in a low-density ($\sim 10^{11}$ cm^{-3}) cesium vapor [13]. Pumping within the $F = 4$ ground-state Zeeman sublevels is achieved indirectly, as a consequence of optical pumping within the $F = 3$ state, off-resonant population pumping from the $F = 3$ to the $F = 4$ state, and SECs [Fig. 1(a)]. Continous indirect pumping transfers about 80% of the atomic population into the stretched state.

This paper explores how this indirect pumping scheme can also be applied to the geometry of a quantum nondemolition arrangement of an atomic magnetometer [14]. This is realized by the implementation of an amplitude-modulated indirect pumping scheme in an atomic sample exposed to a static magnetic field, perpendicular to the propagation of the probe beam [Fig. 1(b)] [15].

One way to describe the atomic system is with the introduction of the collective spin ($\hat{F} = \sum_{i=1}^{N} \hat{f}^{(i)}$, where N is the number of atoms and $\hat{f}^{(i)}$ is the total angular momentum operator of the ith atom) [11]. The stationary spin component along the quantization axis (defined by the magnetic field direction B marked with the green in Fig. 2) is set by the population distribution of the atoms among the Zeeman sublevels, while the oscillating components orthogonal to the axis represent ground-state coherences. Detection of the atomic spin (red arrow in Fig. 2) is realized by a Faraday-type rotation of the light polarization measurement [16–18]. This works by having a probe beam with linear polarization, which propagates along the y axis. As the σ_+ and σ_- components pick up a differential phase shift proportional to F_y, the probe beam will thus emerge from the sample with its linear polarization rotated in proportion to F_y.

Continuous indirect pumping [13] generates a collective atomic spin along a static magnetic field direction [z axis in Fig. 2(a)]. To monitor the atomic spin buildup, a weak radio-frequency (rf) magnetic field was applied to the atomic sample in a direction perpendicular to the static magnetic field. This created a spin component orthogonal to the static magnetic field, which led to precession of the collective spin around that field direction [Fig. 2(a)]. Amplitude-modulated optical pumping along the z axis in Fig. 2(b) simultaneously creates spin components parallel and orthogonal to the static magnetic field. The similarity between the geometries for the cases shown in Figs. 2(a) and 2(b) implies that the combination of SECs and optical pumping will lead to comparable results in those situations.

The sensitivity of the atomic magnetometer, for a given probe beam power, is set by efficiency of the pumping, understood as creating high amplitude of the atomic coherence without affecting its lifetime [19]. We will show that the magneto-optical-rotation signal amplitude (this reflects the ground-state coherence amplitude) as well as the linewidth (set by the SEC coherence relaxation) depend on both the direction (*measurement geometry*) and strength (*measurement dynamics*) of the magnetic field. So far studies of the dependence of the signal amplitude on the measurement geometry have been reported for the case of linearly polarized pump and probe beams (generation of atomic alignment) [20]. In our case, the amplitude-modulated indirect pumping of atomic coherences in the $F = 4$ state involves a circularly polarized pump beam and combines an optical excitation within the $F = 3$ state, off-resonant coherence transfer from the $F = 3$

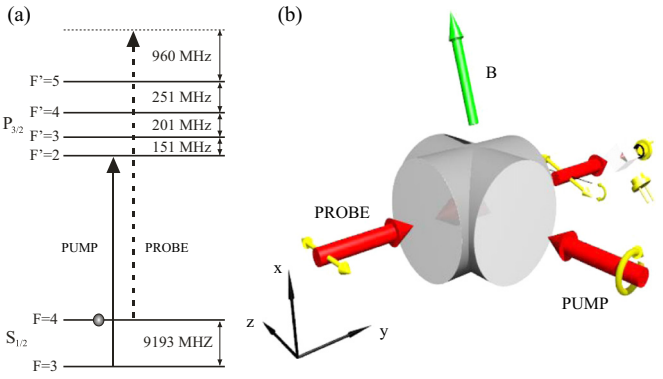

FIG. 1. (Color online) (a) Cesium $6^2S_{1/2} \rightarrow 6^2P_{3/2}$ transition ($D2$ line) energy structure. The arrows represent the frequency of the laser beams used in the experiments (solid, pump, and dotted, probe). (b) Geometry of the experiment. A circularly polarized light beam propagating along the z axis optically pumps the sample of Cs atoms. A linearly polarized probe beam propagates along the y direction. The polarization of the probe light is parallel to the z direction. The polarization state of the light after traversing the atomic sample is measured with a balanced polarimeter. The weak field B is oriented in the xz plane.

to the $F = 4$ state, and SECs. The change in the linewidth and hence the derived SEC decoherence, for the case of changing measurement geometry, can be intuitively explained in terms of a change in the population distribution (and coherence) according to the angle between the static magnetic field and the pump beam propagation axis. The change in the SEC relaxation, for the case of changing measurement dynamics, is related to the time required by SECs (and indirect pumping) to establish an equilibrium in the population distribution and reflects the variation of the mean value of the angular momentum averaged over this time with Larmor precession.

The studies described here are part of the effort to build an atomic magnetometer with $\mathrm{fT/Hz^{1/2}}$ sensitivity able to operate in a nonzero-magnetic-field environment. The best performance of atomic magnetometers has been achieved in

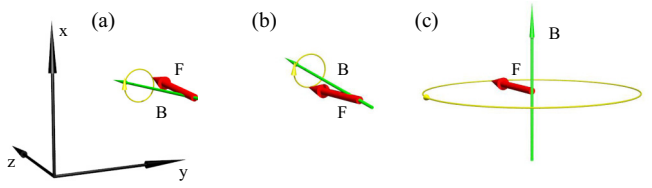

FIG. 2. (Color online) Evolution of the atomic collective spin state F (red arrow) in the presence of a static magnetic field B (defining the quantization axis, green arrow). (a) Configuration of rf spectroscopy experiment. A circularly polarized laser beam pumps atoms along the direction of the static magnetic field (z axis). A weak rf magnetic field generates a spin component orthogonal to the magnetic field (atomic ground-state coherence), which leads to precession of the collective spin vector around the z axis. (b) A circularly polarized laser beam pumps atoms along the z axis. The presence of the magnetic field directed in the xz plane results in the precession of the collective spin vector. (c) Precession of the atomic spin in a magnetic field along the x axis.

systems operated in the so-called spin-exchange relaxation-free (SERF) mode [1] but the operation of SERF magnetometers is limited to very small magnetic fields (below nanotesla) [14,21]. Most real-life measurement scenarios, even in a magnetically shielded environment, include the presence of a small background field (e.g., 100 nT in a standard magnetoencephalography room) that makes the SERF configuration difficult to implement [22–25]. The amplitude-modulated indirect optical pumping scheme described in this paper will allow atomic magnetometers to achieve their highest sensitivities, even in the presence of small background fields.

II. EXPERIMENTAL SETUP

The experimental setup is represented schematically in Fig. 1(b). A sample of thermal Cs atoms is housed in an antirelaxation, paraffin-coated, cross-shaped glass cell (diameter of 22 mm, arm length of 22 mm), with a stem containing metal droplets attached to the center of the cross. A weak dc magnetic field is generated by two pairs of coils (relative field inhomogeneity 0.2%). The line broadening caused by magnetic field gradients has been determined and subtracted from the data presented here. The ambient magnetic field is suppressed by the use of five layers of cylindrical shields made from 2-mm-thick μ-metal with end caps (static shielding better than 3×10^6). The pump beam is generated by a diode laser, frequency locked to the cesium $6^2S_{1/2}\ F = 3 \rightarrow 6^2P_{3/2}\ F' = 2$ transition ($D2$ line, 852 nm). The probe beam is provided by a tapered amplifier, frequency stabilized to the $6^2S_{1/2}\ F = 4 \rightarrow 6^2P_{3/2}\ F' = 5$ transition, and subsequently frequency shifted by 960 MHz to the blue by two acousto-optic modulators in a double-pass configuration [Fig. 1(a)]. The experiment was performed with the probe beam power sufficiently low that it had no noticeable effect on the coherence lifetime. The diameter of the pump and probe beams is approximately 20 mm. The probe light transmitted through the cell is analyzed by a polarimeter and processed by a lock-in amplifier. We are using optical pumping of atoms with amplitude modulation of the pump laser beam (pulse duty cycle 8%–12%) synchronized with the Larmor precession [26,27].

III. RESULTS AND INTERPRETATION

Rf spectra (see Ref. [28] and references therein) are used as a reference for the discussion of the amplitude-modulated indirect pumping. They are recorded under the same experimental conditions (atomic density, probe beam power, pump beam power) as the results presented in the rest of this paper. The main properties of indirect pumping in rf spectroscopy are briefly recalled in Sec. III A, while Sec. III B contains the general properties of the spectral profiles recorded in experiments with amplitude-modulated indirect pumping. Section III C contains results and discussion regarding measurement geometry and Sec. III D regarding measurement dynamics. The results presented in the measurement geometry section provide insight into the dynamics of the pumping process (periods with optical excitation on). The observations discussed in the measurement dynamics section are related to the system evolution in periods with and without optical excitation.

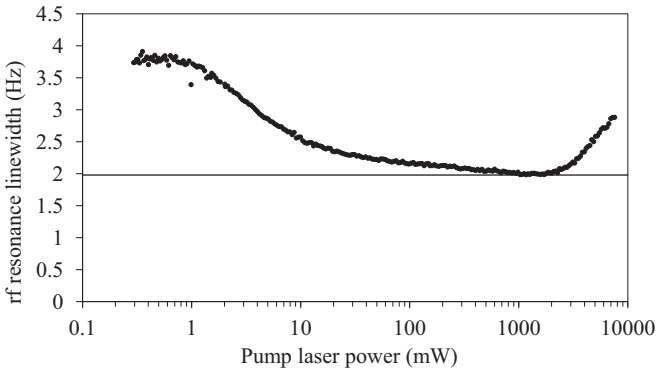

FIG. 3. Width of rf resonance observed for the $F = 4$ manifold versus pump laser power (static magnetic field 1.86 μT). Experimental signals were measured for 10 μW probe laser power and 0.8×10^{11} cm^{-3} atomic density. The black line marks the value of $\Delta\omega_0$, i.e., the minimum value of the linewidth recorded in rf spectroscopy.

A. Continuous indirect pumping in rf spectroscopy

The rf spectrum reveals the change of the magneto-optical-rotation signal as the frequency of a weak rf magnetic field is scanned across the transition frequencies between ground-state Zeeman sublevels of the atoms from a sample placed in a static magnetic field [Fig. 2(a)]. The rf magnetic field couples together neighboring Zeeman sublevels and generates the coherences between them. The linewidths of the rf spectral profiles are defined by the lifetimes of these ground-state coherences. Figure 3 presents the dependence of the linewidths (full width at half maximum) of the rf spectrum components on the pump laser power recorded at 1.86 μT static magnetic field (Larmor frequency $\omega_L = 6.5$ kHz). The particular choice of ω_L (along with the difference in Landé g factors between the $F = 3$ and $F = 4$ ground states) enables a spectral separation of the spectrum components generated by atoms in $F = 3$ and $F = 4$. Consequently, changes in the amplitude and linewidth of both components with pump laser power could be monitored independently (here the focus is only on the $F = 4$ component linewidth). The resonant frequencies of all the Zeeman coherences from each manifold are degenerate because the nonlinear part of the Zeeman shift is negligible. Due to coherence transfer, the linewidths of these components could be characterized by a single value, namely, the linewidth of the strongest component in the rf spectrum [4]. As discussed in [4] the rf profile linewidth does not change significantly below $\omega_L = 100$ kHz.

The SEC contribution to the indirect pumping process depends on the pump laser power and is qualitatively different in low- and high-power ranges (below and above 1 μW) [13]. A pumping within the $F = 4$ state in the low-pump-power range is achieved by SEC-driven replication of the imbalance in the population distribution created by optical pumping within the $F = 3$ manifold. Far-detuned pump light neither pumps atoms within the $F = 4$ manifold nor induces transfer between $F = 3$ and $F = 4$ states. For high-pump-laser powers off-resonant excitations (through $6\,^2S_{1/2}\ F = 3 \rightarrow 6\,^2P_{3/2}\ F' = 3, F' = 4$ transitions) induce depletion of $F = 3$. These excitations combined with optical pumping within the $F = 3$ state contribute to the population imbalance within the $F = 4$ manifold (because of the value of the Clebsh-Gordan coefficients atoms excited to $F' = 3, m = -3$ mostly decay to the $F = 4, m = -4$ sublevel). It is important to stress that the role of the SECs in this pump power range is different from that in the low-pump-power range. Here SECs mostly induce $F = 4 \rightarrow \mathrm{F} = 3$ transfers for all sublevels except $m = -4$ (the stretched state is not fully immune from SECs because of nonzero population in the other Zeeman sublevels). This transfer combined with the optical pumping described before (namely, optical pumping within $F = 3$ and off-resonant transfer $F = 3 \rightarrow F = 4$) creates a recycling mechanism that further contributes to the increase of the $F = 4, m = -4$ population. Thus, the narrowing of the rf spectrum above 1 μW (Fig. 3) results from a high population of the $F = 4, m = -4$ sublevel (light narrowing). The efficiency of the indirect pumping process defined by the ratio of the signal amplitude to the linewidth could not be significantly improved by the introduction of another laser, e.g., operating at $6\,^2S_{1/2}\ F = 4 \rightarrow 6\,^2P_{1/2}\ F' = 4$ transition (as pointed out in Ref. [12], one could achieve a higher population of the stretched state but it results in a decrease of the signal amplitude and broadening of the rf spectral profile). We are going to refer to the minimum value of the linewidth observed in rf spectroscopy as $\Delta\omega_0$.

B. Magneto-optical-rotation signal

Figure 4 presents the magneto-optical-rotation signal (solid black line) recorded as a function of the frequency of the pump laser amplitude modulation. The resonance in signal amplitude is observed when the frequency of the modulation is equal to the atomic spin Larmor precession frequency. The spectral profile consists of two components generated by atoms in the $F = 3$ and $F = 4$ states. The dotted red line in Fig. 4 shows a fit with two Lorentzian profiles, each represented by dashed blue lines. Because of optical pumping within the $F = 3$ state, the linewidth of the $F = 3$ component is prone to

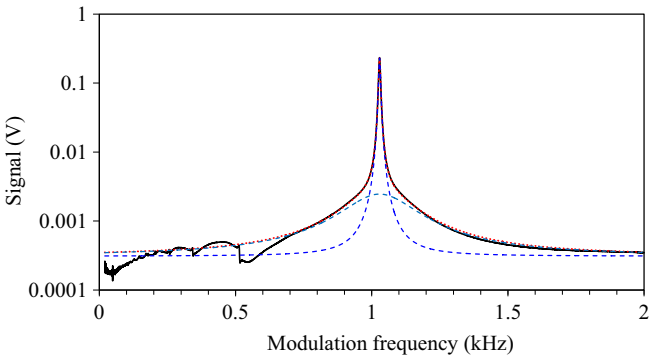

FIG. 4. (Color online) The magneto-optical-rotation signal recorded as a function of the frequency of pump laser amplitude modulation (solid black line). The fit is marked by the dotted (red) line while the two individual Lorentzian components of the fit are shown with the dashed (blue) lines. The experimental signal was measured for 100 μW probe laser power, 2900 μW pump laser power amplitude modulated with an 8% duty cycle, and 0.3×10^{11} cm^{-3} atomic density.

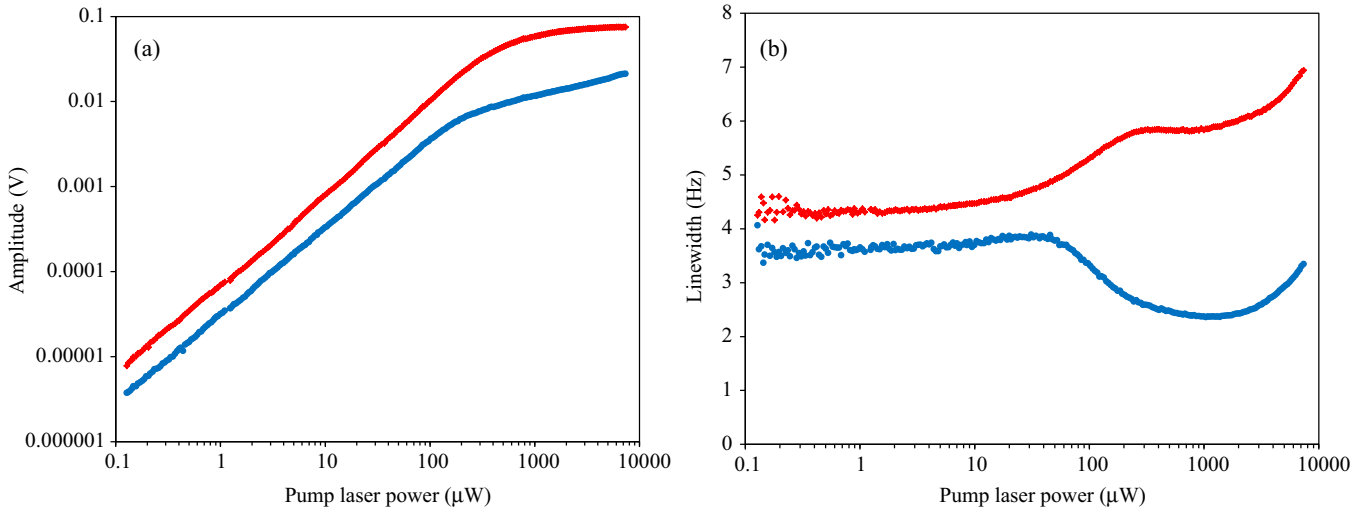

FIG. 5. (Color online) Dependence of the amplitudes (a) and widths (b) of spectral profiles for amplitude-modulated indirect pumping on the pump beam power for two values of the angle between the direction of the magnetic field and z axis (10°, blue dots; 75°, red diamonds). Experimental signals were measured for 10 μW probe laser power and 0.8×10^{11} cm^{-3} atomic density.

power broadening. Moreover, due to the probe laser detuning [Fig. 1(a)] the amplitude of that component is more than an order of magnitude smaller than that produced by atoms in $F = 4$. In the following parts the discussion is focused only on the narrower, $F = 4$, component. The signal created by atoms in $F = 4$ has eight degenerate subcomponents created by coherences between neighboring Zeeman sublevels of the $F = 4$ state. The amplitude of the subcomponent is proportional to the strength, while the linewidth represents the lifetime of the particular coherence. Within the relevant magnetic field range ($\omega_L \leqslant 1$ kHz) [29] the linewidths of all the components are equal (set by the coherence transfer within the $F = 4$ state) and reflect the linewidth of the $-4 \leftrightarrow -3$ coherence (the leading component in the signal) [4].

Apart from the major peak at $\omega_L = 1.029$ kHz the spectrum in Fig. 4 shows resonances at $\frac{1}{2}\omega_L = 0.5015$ kHz, $\frac{1}{3}\omega_L = 0.343$ kHz, and $\frac{1}{4}\omega_L = 0.25$ kHz, etc. Similarly to the main peak, each of these peaks contains a narrow and a broad component [21]. The resonances result from the fact that we use a square pulse to modulate the pump beam amplitude. The resonances occur when the frequencies of the individual Fourier components of optical excitation modulation (multiples of the modulation frequency) match ω_L [30]. We have confirmed the presence of these resonances in separate measurements, where the pump amplitude modulation frequency was scanned around $\frac{1}{2}\omega_L$ ($\frac{1}{4}\omega_L$), while the signal was recorded by a lock-in amplifier referenced to ω_L.

C. Amplitude-modulated indirect pumping: Measurement geometry

Figures 2(b) and 2(c) show two boundary cases of the generic configuration discussed in this section, i.e., a static magnetic field in the xz plane. The particular case shown in Fig. 2(c) will be considered in Sec. III D. Although detailed theoretical modeling is beyond the scope of this paper, we present intuitive geometric arguments that provide insight into most of the results shown. It can be shown with basic calculations that in the case presented in Fig. 2(b) (high population imbalance) atomic coherences are generated between the pairs of Zeeman sublevels of the $F = 4$ level with m close to the minimum or maximum value. This results in a narrowing of the linewidth of the $-4 \leftrightarrow -3$ coherence and observed spectral profile. On the other hand, in the configuration shown in Fig. 2(c) (no population imbalance) optical excitation creates coherences between all neighboring Zeeman sublevels, which will manifest itself in an increased relaxation of the $-4 \leftrightarrow -3$ coherence. This means that the standard formulation of the light narrowing effect for the case of rf resonances (reduction of the linewidth with increased population imbalance) holds for the case discussed in this paper.

Figure 5(a) shows two data sets representing the dependence of the amplitudes of the spectral profiles in amplitude-modulated indirect pumping on the pump laser power recorded for two values of the angle α between the magnetic field and the z axis (blue dots, $\alpha = 10°$; red diamonds, $\alpha = 75°$). It shows that, for both values of α, the amplitude of the signal grows with pump laser power and reaches a maximum level around 10 mW. As mentioned before, the difference between the two cases is the character of the optical excitation: for the case of $\alpha = 10°$ the excitation primarily builds up population imbalance, while for $\alpha = 75°$ it mainly generates coherences within the $F = 3$ manifold. In both cases, for the pump power below 60 μW, the coherences created optically within $F = 3$ are transferred to the $F = 4$ manifold by SECs. This explains the same rate of signal amplitude increase observed for both data sets in the low-pump-power range. Above 100 μW, off-resonant pumping from $F = 3$ to $F = 4$ starts. In the first case ($\alpha = 10°$, blue dots), it transfers mostly population, which does not increase the coherence amplitude, while for the other case, it directly creates coherences in the $F = 4$ state. This causes the difference in signal amplitude growth rates in the high-pump-power regime, shown in Fig. 5(a).

Figure 5(b) shows the dependence of the corresponding linewidths on the pump laser power (blue dots, $\alpha = 10°$;

red diamonds, $\alpha = 75^\circ$). For $\alpha = 10^\circ$ a constant linewidth is observed up to 60 μW, followed by line narrowing in the 50-2000 μW range. The broad minimum is reached at about 1500 μW, while for the higher pump powers a gradual increase of the linewidth is observed. The similarities between this data set and that shown in Fig. 3 confirm that in both cases we observe a light narrowing effect and demonstrate that SECs play the same role in amplitude-modulated indirect pumping as that described in Sec. III A. We have performed the observations of the spectral profiles with amplitude-modulated optical pumping involving two lasers: one operating at the $6^2S_{1/2}\ F = 4 \rightarrow 6^2P_{1/2}\ F' = 4$ and the other at the $6^2S_{1/2}\ F = 3 \rightarrow 6^2P_{3/2}\ F' = 4$ transition [11]. The results confirmed that the efficiency of the pumping from that measurement was worse than for the amplitude-modulated indirect pumping with one laser.

The linewidth dependence on the pump beam power recorded at $\alpha = 75^\circ$ has a different character. The offset between the two data sets in Fig. 5(b) in the low-pump-power regime results from difference in the population imbalance (spin component along the magnetic field) that affects the linewidth of the $-4 \leftrightarrow -3$ coherence and causes its higher value. Although the $\alpha = 75^\circ$ data set is similar to the $\alpha = 10^\circ$ case below 60 μW, in the power range 200–2000 μW the profile narrowing is masked by a gradual increase of the linewidth. The pump laser simultaneously couples to all Zeeman sublevels within the $F = 3$ state and increasing the pump laser power decreases any population difference among the different Zeeman sublevels. Because the $-4 \leftrightarrow -3$ coherence relaxation rate depends on population imbalance, this leads to a decoherence increase.

Figure 6 (black dots) shows the results of a systematic measurement of the amplitude (a) and linewidth (b) of the spectral profile dependence on α (the amplitude of the magnetic field was kept constant over the course of this measurement, giving a 1 kHz Larmor frequency). Change in the angle between 0 and 90° is equivalent to the transition from the configuration depicted in Fig. 2(b) to that in Fig. 2(c). There are three mechanisms that contribute to the angular dependence of the signal amplitude. The first two are related to the change of the character of the optical excitation with the tilt of the magnetic field. For $\alpha = 0^\circ$ the excitation creates solely population imbalance, while for $\alpha = 90^\circ$ it generates atomic coherences in the $F = 3$ manifold. Thus the tilt of the magnetic field causes a change in the amplitude of the $F = 3$ atomic coherence signal $\sim\sin\alpha$ [31]. As discussed before, the transfer of the coherences between the $F = 3$ and the $F = 4$ states involves SECs (no angular dependence) and off-resonant excitation, with the efficiency scaling as $\sim\sin\alpha$ [32]. The dashed red line shows the combined contribution from these mechanisms to the angular dependence of the signal amplitude ($\sim\sin\alpha + \sin^2\alpha$) [33]. The third mechanism is related to the change in the spectral profile linewidth with the amplitude of the vertical magnetic field component (measurement dynamics). Changes of the linewidth with α, shown in Fig. 6(b), reflect the change in efficiency of the light narrowing (i.e., the generation of population imbalance) with α. The efficiency of the population imbalance generation varies as $\cos\alpha$, and consequently the linewidth value changes scale as $\sin\alpha$ [dashed red line in Fig. 6(b)]. The linewidth values recorded for angles less than 40° fall below those expected from geometrical considerations. This results from the change of the linewidth with the amplitude of the vertical component of the magnetic field (measurement dynamics) and will be discussed in the following section. The contribution (scaled) to the angular dependence of the signal amplitude reflecting

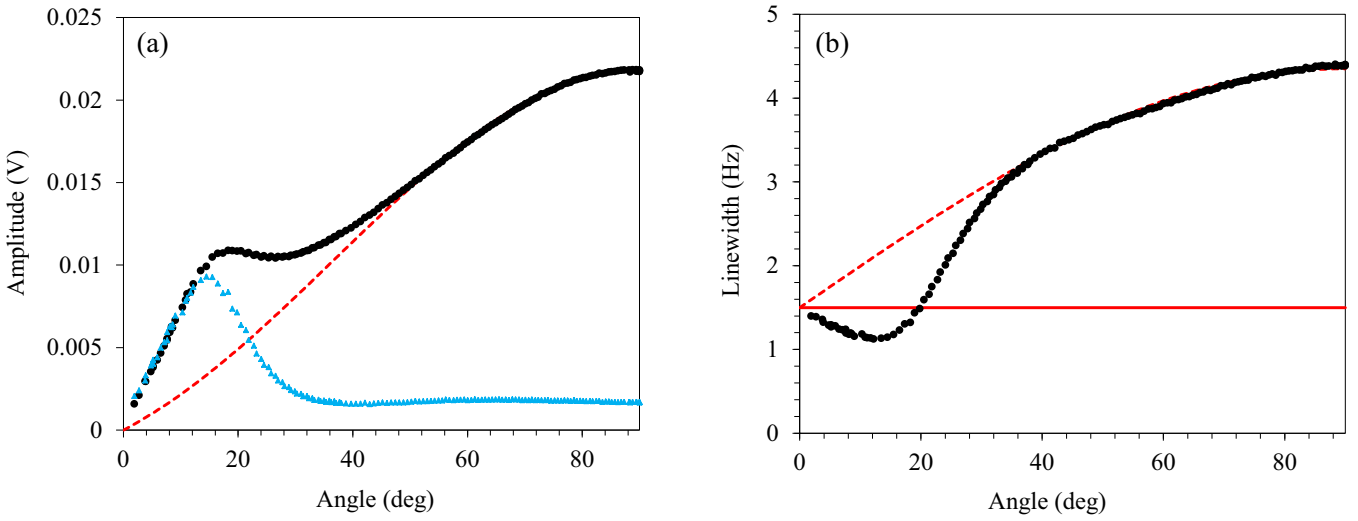

FIG. 6. (Color online) Dependence of the amplitudes (a) and widths (b) of the spectral profiles (black dots) for amplitude-modulated indirect pumping on the angle between the magnetic field and the pump beam propagation direction (z axis). The amplitude of the magnetic field was kept constant over the course of this measurement to give a Larmor frequency of 1 kHz. The dashed red curve in (a) shows modifications of the signal amplitude caused by the change of character of the optical excitation, while blue triangles show the contribution from line narrowing. The dashed red line in (b) shows the changes to the linewidth resulting from geometrical considerations, while the solid red line represents the value of $\Delta\omega_0$, i.e., the minimum value recorded in rf spectroscopy at the same atomic density. Experimental signals were measured for a 1500 μW pump laser power amplitude modulated with 8% duty cycle, 10 μW probe laser power, and 0.33×10^{11} cm^{-3} atomic density.

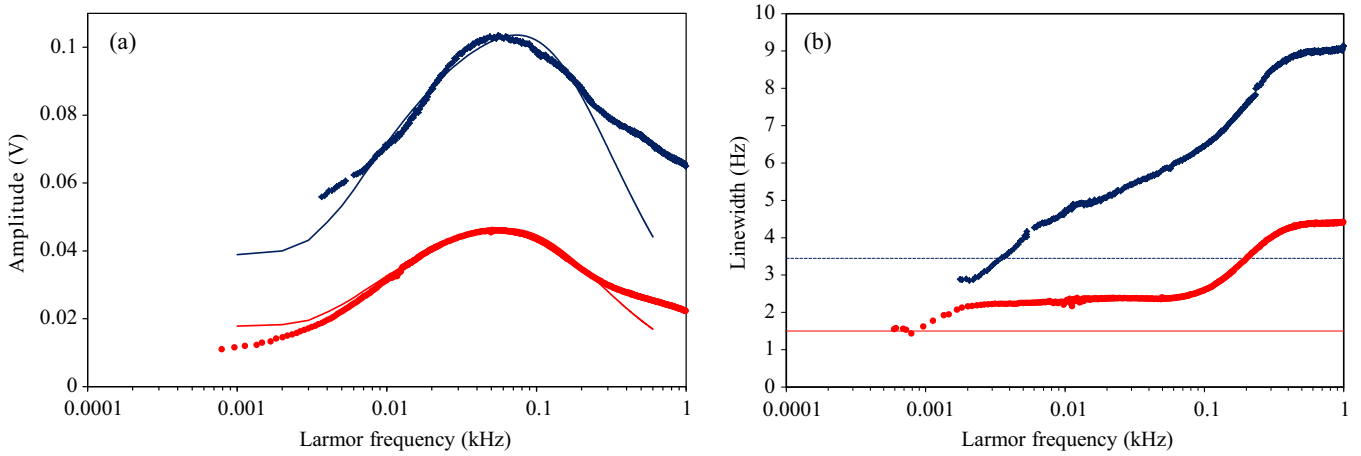

FIG. 7. (Color online) Dependence of the amplitudes (a) and widths (b) of spectral profiles for amplitude-modulated indirect pumping on the amplitude of the magnetic field (in terms of the Larmor precession frequency) directed along the x axis. Experimental signals were measured for a 1500 μW pump laser power amplitude modulated with a 12% duty cycle, 10 μW probe laser power, and 0.33×10^{11} cm^{-3} (red dots) and 1.2×10^{11} cm^{-3} (blue diamonds) atomic densities. Solid red and dashed blue lines (b) represent the value of $\Delta\omega_0$, i.e., the minimum value recorded in rf spectroscopy at the same atomic density.

the change of the linewidth due to measurement dynamics is shown with blue triangles in Fig. 6(a).

Figure 6(b) shows the important difference of the pumping considered in this paper compared with standard SERF measurements [21], where the linewidth of the spectral profile increases with the absolute strength of the magnetic field. The results discussed in this section show that even for a relatively high magnetic field ($\omega_L = 1$ kHz) it is possible to observe (for $\alpha < 20^\circ$) spectral profiles with the linewidth $\sim\Delta\omega_0$.

D. Amplitude-modulated indirect pumping: Measurement dynamics

Figure 7 shows the dependence of the amplitude (a) and linewidth (b) of the spectral profile on the amplitude of a magnetic field directed along the x axis (components of the magnetic field in the zy plane were compensated). The configuration of the measurements reflects the collective spin evolution shown in Fig. 2(c). In that case the pump laser excites solely coherences between the Zeeman sublevels of the $F = 3$ state. The plots show two sets of data recorded at 0.33×10^{11} cm^{-3} (red dots) and 1.2×10^{11} cm^{-3} (blue diamonds) atomic densities. The dependence of the spectral profile amplitude on the magnetic field strength reflects the fact that measurement of the amplitude of the atomic coherence oscillations averages over the stages with and without optical excitation. Figure 8 shows one period of the spin precession consisting of the pumping stage, in which the atomic collective spin undergoes a relatively fast buildup process followed by a relaxation in the absence of the pump beam (the amplitude of the coherence is marked with a red solid line). For low values of ω_L, averaging includes a relatively long stage without any signal and a reduction of the length of this stage (by increasing ω_L) leads to an increase in the spectral profile amplitude. Figure 8 shows that reduction of the precession period, and consequently the length of the optical excitation, does not necessarily affect the efficiency of the pumping process. However, for the case of very high ω_L the pumping efficiency is affected by the length of the precession period. Thus one can expect an optimum balance between these two factors (signal buildup and relaxation), which is manifested by the maximum in Fig. 7(a). It is worth pointing out that the Larmor frequency, for which the maximum is observed does not change with atomic density. This shows that SECs contribute to the pumping and relaxation processes. The solid lines in Fig. 7(a) show the results of simple amplitude modeling based on the signal evolution presented in Fig. 8.

The two data sets in Fig. 7(b) show the same generic tendency, i.e., an increase of the linewidth with increasing Larmor precession frequency. For the case with atomic density 1.2×10^{11} cm^{-3}, the linewidth growth is gradual, while the other shows a plateau in the Larmor frequency range 2–60 Hz followed by an increase. The fact that for low frequencies the dependencies reach the value of $\Delta\omega_0$ (marked with solid red and dashed blue lines) means that SECs enhance the amplitude-modulated pumping process. This indicates that for the case of slow precession, the rate of SECs is high enough that an equilibrium in terms of SEC-driven changes in atomic collective spin could be established (i.e., SEC changes in atomic collective spin adiabatically follow spin precession). It is particularly important in the high-pump-power region (above 60 μW), where, as already mentioned, observation of light narrowing relies on partial immunity of the atomic

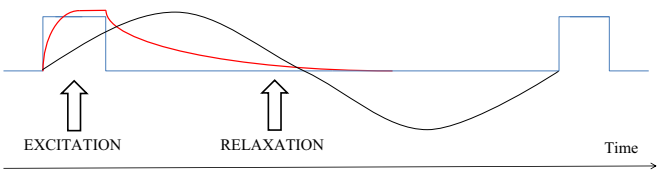

FIG. 8. (Color online) Two phases in the course of a single period of the atomic spin precession: Optical excitation, marked by two square pulses, creates the atomic coherence (the amplitude is marked with a red solid line) and the atomic coherence relaxation in the absence of the pump light.

coherences involving the stretched state to SECs in the recycling process. The change of the linewidth as a function of the vertical magnetic field amplitude ($\omega_L < 300$ Hz) accounts for the departure of the angular dependence of the amplitude and width from the simple model based solely on geometrical considerations (dashed red curves in Fig. 6).

For $\omega_L \sim \Delta\omega_0$ we observed an asymmetry in spectral profiles. The line shape modifications for $\omega_L < \Delta\omega_0$ are a topic for future studies.

IV. CONCLUSIONS

We have experimentally explored the roles of measurement geometry and dynamics on amplitude-modulated indirect pumping. We have discussed the necessary conditions for observing light narrowing. In particular we have shown that for the low-Larmor-frequency range ($\omega_L \leqslant 10$ Hz) SEC-driven changes in atomic spin adiabatically follow the spin precession and SECs contribute to amplitude-modulated indirect pumping (in particular light narrowing), while for higher frequencies SECs start to increase the system decoherence.

The geometry studied in the presented experiments is the same as in dc atomic magnetometers operating in a quantum nondemolition configuration [14]. This configuration (with the probe laser beam orthogonal to the magnetic field being measured) enables an evasion of probe beam backaction, which contributes to the noise level. Consequently we envisage the opportunity of getting the signal-to-noise ratio, even at this relatively low density (10^{11} cm^{-3}), on the order of 10^6, limited only by the standard quantum limit. An additional advantage of implementation of the quantum nondemolition configuration is an increase in the measurement bandwidth that results from the fact that both the signal and the noise (defined by atomic projection noise) have the same spectral characteristics [28] (i.e., the signal-to-noise ratio does not change dramatically with frequency as long as the noise is defined by atomic projection noise).

The Larmor frequency range explored in the studies covers not only the near-zero range, which is the usual domain of atomic magnetometers in SERF mode, but also higher Larmor frequencies, where operation of the SERF magnetometers suffers from the increased SEC decoherence (and consequently reduced sensitivity). It is worth pointing out in this context that the increase of the linewidth in this Larmor frequency range is on the order of 3, compared to a factor of 100 for the case of SERF magnetometers [14,21]. Relatively low linewidths of the observed profiles combined with high signal-to-noise ratio create the opportunity to perform precise magnetic field measurement (at the fT/Hz$^{1/2}$ level) above the so-called zero-magnetic-field regime.

ACKNOWLEDGMENTS

The work was funded by the U.K. Department for Business, Innovation and Skills as part of the National Measurement System Programme.

[1] I. K. Kominis, T. W. Kornack, J. C. Allred, and M. V. Romalis, Nature (London) **422**, 596 (2003).
[2] W. Happer and H. Tang, Phys. Rev. Lett. **31**, 273 (1973).
[3] W. Happer and A. C. Tam, Phys. Rev. A **16**, 1877 (1977).
[4] W. Chalupczak, P. Josephs-Franks, B. Patton, and S. Pustelny, Phys. Rev. A **90**, 042509 (2014).
[5] N. D. Bhaskar, J. Camparo, W. Happer, and A. Sharma, Phys. Rev. A **23**, 3048 (1981).
[6] S. Appelt, A. B. Baranga, C. J. Erickson, M. Romalis, A. R. Young, and W. Happer, Phys. Rev. A **58**, 1412 (1998).
[7] S. Appelt, A. B. Baranga, A. R. Young, and W. Happer, Phys. Rev. A **59**, 2078 (1999).
[8] I. M. Savukov and M. V. Romalis, Phys. Rev. A **71**, 023405 (2005).
[9] S. J. Smullin, I. M. Savukov, G. Vasilakis, R. K. Ghosh, and M. V. Romalis, Phys. Rev. A **80**, 033420 (2009).
[10] W. Wasilewski, K. Jensen, H. Krauter, J. J. Renema, M. V. Balabas, and E. S. Polzik, Phys. Rev. Lett. **104**, 133601 (2010).
[11] B. Julsgaard, J. Sherson, J. L. Sorensen, and E. S. Polzik, J. Opt. B **6**, 5 (2004).
[12] W. Chalupczak, P. Josephs-Franks, R. M. Godun, and S. Pustelny, Phys. Rev. A **88**, 052508 (2013).
[13] W. Chalupczak, R. M. Godun, P. Anielski, A. Wojciechowski, S. Pustelny, and W. Gawlik, Phys. Rev. A **85**, 043402 (2012).
[14] V. Shah, G. Vasilakis, and M. V. Romalis, Phys. Rev. Lett. **104**, 013601 (2010).
[15] W. E. Bell and A. L. Bloom, Phys. Rev. Lett. **6**, 280 (1961).
[16] Y. Takahashi, K. Honda, N. Tanaka, K. Toyoda, K. Ishikawa, and T. Yabuzaki, Phys. Rev. A **60**, 4974 (1999).
[17] G. A. Smith, S. Chaudhury, and P. S. Jessen, J. Opt. B **5**, 323 (2003).
[18] J. M. Geremia, J. K. Stockton, and H. Mabuchi, Phys. Rev. A **73**, 042112 (2006).
[19] The pump beam affects neither the level of photon shot noise in detection nor the amplitude of the atomic projection noise.
[20] S. Pustelny, W. Gawlik, S. M. Rochester, D. F. Jackson Kimball, V. V. Yashchuk, and D. Budker, Phys. Rev. A **74**, 063420 (2006).
[21] M. P. Ledbetter, I. M. Savukov, V. M. Acosta, D. Budker, and M. V. Romalis, Phys. Rev. A **77**, 033408 (2008).
[22] O. Katz, M. Dikopoltsev, O. Peleg, M. Shuker, J. Steinhauer, and N. Katz, Phys. Rev. Lett. **110**, 263004 (2013).
[23] X. Xia, A. Ben-Amar Baranga, D. Hoffman, and M. V. Romalis, Appl. Phys. Lett. **89**, 211104 (2006).
[24] C. Johnson, P. D. D. Shwindt, and M. Weisend, Appl. Phys. Lett. **97**, 243703 (2010); Phys. Med. Biol. **58**, 6065 (2013).
[25] T. H. Sander, J. Preusser, R. Mhaskar, J. Kitching, L. Trahms, and S. Knappe, Biomed. Opt. Express **3**, 981 (2012).
[26] W. Gawlik, L. Krzemien, S. Pustelny, D. Sangla, J. Zachorowski, M. Graf, A. O. Sushkov, and D. Budker, Appl. Phys. Lett. **88**, 131108 (2006).
[27] S. Pustelny, A. Wojciechowski, M. Gring, M. Kotyrba, J. Zachorowski, and W. Gawlik, J. Appl. Phys. **103**, 063108 (2008).
[28] D. Budker and D. F. Jackson Kimball, *Optical Magnetometry* (Cambridge University Press, Cambridge, 2013).

[29] The studies presented in this paper are limited to the Larmor frequency range 0–1 kHz. (1) This represents the highest level of magnetic background in magnetoencephalography rooms. (2) We observed changes in SEC relaxation rates only for $\omega_L \leqslant 1$ kHz.

[30] Z. D. Grujic and A. Weis, Phys. Rev. A **88**, 012508 (2013).

[31] A formal derivation of the angular dependence of the ground-state coherence amplitude can be found in R. Wynands, A. Nagel, S. Brandt, D. Meschede, and A. Weis, Phys. Rev. A **58**, 196 (1998).

[32] For $\alpha = 0^\circ$ off-resonant excitation transfers solely population between the $F = 3$ and $F = 4$ ground states, while for $\alpha = 90^\circ$ it transfers ground-state coherence.

[33] We have also observed the dependence of the amplitudes of the spectral profiles on the angle between the magnetic field and the pump beam propagation direction for pump beam power 10 μW. In this power range the atomic coherence is transferred between ground-state manifolds by SECs and the angular dependence of the spectral profile amplitude follows $\sin\alpha$.